Acta Mechanica Sinica
https://doi.org/10.1007/s10409-021-01134-7

RESEARCH PAPER

Scaling analysis of the circulation growth of leading-edge vortex in flapping flight

Yang Xiang[1] · Haotian Hang[2] · Suyang Qin[1] · Hong Liu[1]

Received: 26 May 2021 / Revised: 29 June 2021 / Accepted: 8 July 2021

Abstract
In this paper, an experiment of a robotic model at Reynolds number of approximately 240 is performed with the aim of establishing a scaling law for describing the circulation growth of the leading-edge vortex (LEV) on a flapping wing. Three typical modes of wing rotation, i.e., advanced, symmetric, and delayed modes, are considered to examine the effects of wing rotation on the scaling formation of LEV. The streamwise velocity fields of the LEV along the span of the wing are measured by particle image velocimetry technique. Experimental results demonstrated that a spirally three dimensional (3D) LEV with spanwise distribution of circulation rolls up on the upper surface of wing and the circulation of LEV usually obtains the peak before the end of wing stroke. Based on the concept of vortex formation time, the formation time of the 3D LEV are defined in two distinct manners. One (denoted by T^{*}_{LEV}) is defined based on the LEV circulation, and the other (denoted by T^{**}_{LEV}) is defined based on the wing kinematics. It is found that T^{**}_{LEV} increases monotonously during the upstroke and downstroke, whereas T^{*}_{LEV} generally arrives peaks and then decreases. The peak value of T^{*}_{LEV} indicates the formation number of LEV, which stays in the range of 2.5–5.5, agrees with the scaling formation number predicted by other vortices. Moreover, the mode of wing rotation plays a controllable role in the formation number of LEV by modulating the characteristic length scale that feeds the formation of LEV. After reaching the formation number, the LEVs stably remain attached on the flapping wing and even further grow at some spanwise locations because of vorticity transport. Furthermore, the linear relationship between T^{*}_{LEV} and T^{**}_{LEV} before reaching the formation number can suggest a potential model for predicting the circulation growth of LEV based on wing kinematics.

Keywords Leading-edge vortex · Circulation · Formation number · Scaling formation

1 Introduction

Natural selection for more than 350 million years gives insects unsurpassed flight performance and maneuverability [1,2]. Existing investigations have demonstrated that the generation of high lift is greatly attributed to the formation of leading-edge vortex (LEV) on the wing [3–7]. Understanding the dynamics of LEV has been the source of motivation for many scientists to investigate the formation of LEV [8–11]. However, mathematically modelling the LEV formation is quite difficult, not only because the underlying mechanisms governing the formation of LEV are not entirely understood, but also because the factors effecting the formation of LEV are too many. Without a unified frame work for describing the LEV formation, it is quite challenging, even impossible, to predict the formation, growth, and separation of the LEV and its contribution to the aerodynamic forces of flapping flight.

Since Ellington found the occurrence of the LEV on the wing of flapping flight [12], numerous studies have been conducted to investigate the role of wing kinematics, wing geometries, and Reynolds number in the formation, dynamics, and stability of LEV [13–20], particularly including the comprehensive review [21]. Besides, the roles of the LEV in the generation of high-lift have been also richly investigated [22–24]. The most remarkable characteristic of LEV in flapping flight is that the LEV remains stably attached on the

Executive Editor: Hao Liu.

✉ Suyang Qin
liam_young@sjtu.edu.cn

[1] J.C. Wu Center for Aerodynamics, School of Aeronautics and Astronautics, Shanghai Jiao Tong University, Shanghai 200240, China

[2] School of Aeronautics and Astronautics, Shanghai Jiao Tong University, Shanghai 200240, China

Published online: 31 August 2021

wing, whereas a LEV is shed after a few chord lengths of travelling on a translating two dimensional (2D) airfoil [14]. The underlying mechanisms on the LEV stability are attributed but not limited to spanwise transport, centrifugal and Coriolic accelerations, and wingtip-vortex effects [10,16,25,26]. A mechanism is believed to balance the flux of vorticity transported into the LEV so as to keep the stabilization of LEV on the wing. In spite of the physics of LEV formation, growth, stability, and separation are not entirely understood, some date-driven and mathematic models have been proposed to predict the circulation and separation of LEV [27–31]. Just as Eldredge and Jones [21] pointed out, the models have the potential to provide real-time estimation of the LEV formation, however, the three dimensional three dimensional (3D) LEV models are largely unexplored, which should consider the influence of the tip vortices and the spanwise flow.

Recently, Onoue and Breuer [19,20] analyzed the 3D LEV dynamics on a rapidly pitching plate and the swept/un-swept wings over a wide range of flow condition, and they found that the LEV circulation and formation timescale coincide with the concept of optimal vortex formation number originally originated from the vortex ring formation found by Gharib et al. [32] and generalized by Dabiri [33]. In 1998, Gharib et al. [32] found that vortex rings cannot grow indefinitely but pinch off at a critical formation timescale, termed as formation number $F^* \approx 4.0$. The formation number of vortex rings is explained by the Kelvin-Benjamin variational principle, which characterizes the energy maximum of vortex rings [32–34]. From 1998 up to now, the concept of vortex formation number has been extended to the other canonical vortices including the tip vortex [35], the wake vortex behind a cylinder [36], non-axisymmetric vortex rings, and the LEV generated by pitching and plunging plates [13]. Notably, the formation number of vortex rings generated by the piston-cylinder apparatus can be varied by some parameters, such as the velocity programs of piston [37], temporal-varying exit diameter [38], and compressibility [39,40]. In particular, the formation number of vortex ring can increase up to 8.0, when a temporally decreasing nozzle exit diameter is introduced [38]. The formation number of vortex ring can decrease to 2.0, when the nozzle has a converging geometry [41]. Moreover, the formation number hints the principle of optimal vortex formation, which widely exits in the biological propulsions [33]. As for the LEV, Rival et al. [13,42] found that the circulation growth of the LEV generated by a pitching and plunging plate can be well-described by the principle of optimal vortex formation number. They found that the LEV obtains the maximum scaling circulation and the vortex formation number stay within a narrow range of 3.0–4.0. Moreover, Rival et al. [13], Wong et al. [16], and Onoue et al. [19,20] investigated the formation number of LEV by considering the dependencies on the wing geometries, pivot point location, pitch rate, oscillation amplitude, Reynolds number, and so on. They found that the critical formation number of the LEVs is robust for a wide range of condition. However, the formation of LEVs generated by a pitching and plunging plate/wing is quite different from the formation of LEV generated by a flapping wing. As reviewed above, one of the most remarkable features is that a stable 3D LEV is generated on the flapping wing. Besides, the formation of LEV is strongly influenced by the wing rotation, the Coriolic effects, and the wingtip vortex [11,43]. Therefore, a remained question arises that whether the formation of LEVs generated by flapping wings satisfies the scaling law described by the principle of optimal vortex formation number or not.

As for the flapping flight, wing rotation not only has a great contribution to the high-lift generation, but also plays a significant role in steering maneuvers [44]. By using 3D, high-speed videograph, researchers observed the body motions and wing kinematics of insects during maneuvers including take-off, hovering, forward flight, fast change in flight speed and/or flight direction, and body saccades [44]. In general, the kinematics of wing rotation performs three modes, which is distinguished by the phase δ between stroke reversal and wing rotation [23,44,45]. When the wing rotation precedes stroke reversal, the advanced mode is performed and corresponds to $\delta < 0$. When wing rotation occurs symmetrically with respect to stroke reversal, the corresponding mode is symmetrical and corresponds to $\delta = 0$. The delayed mode $\delta > 0$ is accepted when wing rotation is delayed with respect to stroke reversal. The modes of wing rotation have a significant influence on the formation of LEVs and the generation of aerodynamic forces [4]. However, the influence of wing rotation on the scaling formation number of LEV is unclear and even has never been investigated upon to now to our limited knowledge.

Therefore, the primary objectives for the present study are at least twofold. First, to determine the scaling formation number of the LEV generated by a flapping wing. Second, to examine the influence of wing rotation on the scaling formation number of the LEV. To achieve the objectives, a robotic model is designed in this paper and the time-dependent flow fields of LEV are recorded by particle image velocimetry (PIV) technique.

The rest of this paper is organized as follows. Both the experimental set-up and PIV measurements are introduced in Sect. 2. Then, the results are demonstrated and discussed in Sect. 3, which is further divided into three subsections including evolution of flow pattern around the flapping wing, circulation distribution and evolution of LEV, and scaling formation and formation number of LEV. Section 4 concludes the paper with a brief discussion.

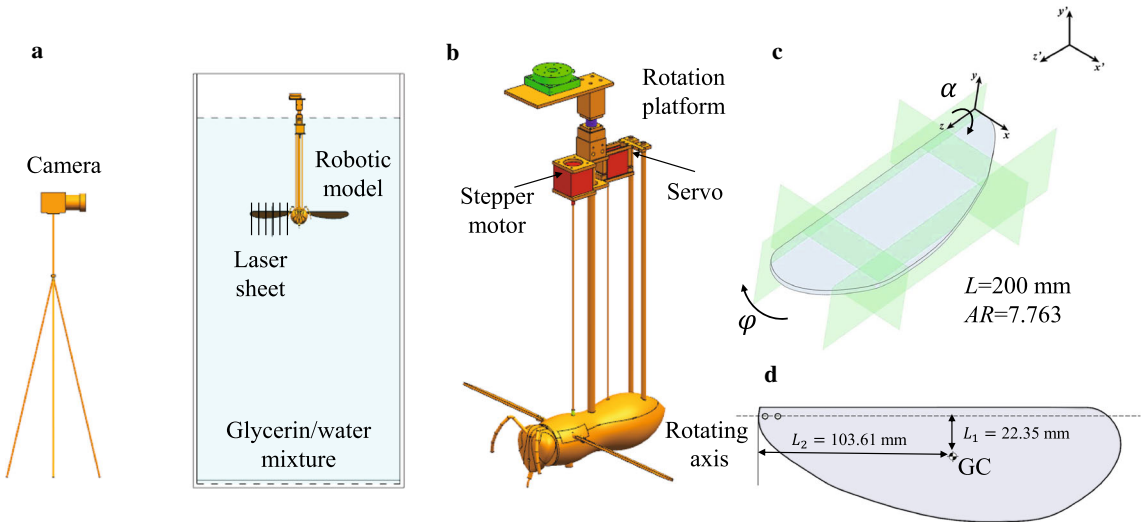

Fig. 1 Experimental set-up. **a** Schematic of experimental set-up and PIV measurements. **b** 3D model of the robotic fly. **c** Shape of the wing and two coordinate systems are applied in this paper. The $x'-y'-z'$ coordinate system is inertial system in lab, the $x-y-z$ coordinate system is a moving system and the origin of this system is at the wing root. z indicates the spanwise direction, and y indicates the direction perpendicular to the wing plane. **d** The planar shape of the wing. GC is the geometric center, the distance from the wing geometric center to the axis of rotation is $L_1 = 103.61$ mm, and the distance from the wing geometric center to the wing root is $L_2 = 22.35$ mm

2 Methods

2.1 Experimental set-up

As shown in Fig. 1a, a robotic model was immersed in a 1.2 m × 1.22 m × 2 m tank filled with glycerin/water mixture (density $\rho = 1.12 \times 10^3$ kg/m^3, kinematic viscosity $\upsilon = 3.8915 \times 10^{-5}$ m^2/s at temperature $T = 20\,^{\circ}$C). The geometry of the tank was designed to minimize potential wall effects by referring to the design of Dickinson et al. [4]. The viscosity of the mixture, the size of the wing, and the flapping frequency of the robotic model were chosen to match the typical Reynolds number of insect flight ($Re \approx 240$). Referring to the studies of Ellington [12] and Dickinson et al. [4], the Reynolds number of hovering flight is defined as

$$Re = \frac{4\phi_0 L^2 n}{\upsilon AR}, \tag{1}$$

where ϕ_0 means the stroke amplitude, L is the span length, n is the flapping frequency, υ is the kinematic viscosity, and AR is the aspect ratio defined as $AR = \frac{4L^2}{S}$ (S is the surface area of the wing). As shown in Fig. 1c, the wing has a span of $L = 200$ mm and the aspect ratio is $AR = 7.763$. The geometry of wing is designed by referring to the shape of a bee [46] and is made of Plexiglas (3 mm thick). The robotic model has a bee-like body installed with one wing on one side. All the components driven the flapping motion of wings are hidden in the inner of the body to avoid affecting flow around the flapping wing. The translation of wing is driven by a servo motor and the rotation of wing is driven by a stepper motor. Coordination of the servo motor and the stepper motor is controlled by a development board called Arduino (MEGA 2560). The body part near the wing's root is made of the elastic rubber. In such situation, the influence of the running mechanisms on the formation of the LEV near the wing's root is minimum.

Digital PIV technique was performed to measure the velocity fields in a slice of fluid centered on the wing. Hollow glass beads with a mean diameter of 50 μm and a density of 1.02 g/cm^3 were chosen as the seeding particles. The particles were illuminated by a 1.5 mm thick laser sheet projected by a continuous laser with 10 W of power and wavelength of 532 nm. A high-speed camera was placed perpendicular to the laser sheet. In the present study, the formation of LEV is the most concerned and is a strongly 3D flow. The direction of the LEV vorticity is spanwise. Thus, the measured plane should be parallel to the $x-y$ plane of the wing and was placed at the spanwise locations along the wing. However, the laser sheet cannot coincide with the measured plane all the time, and the particles will be out of the measured plane when the wing revolves. Hence, the camera was triggered to record only one pair of images at the moment when the measured plane coincides with the laser sheet during one stroke cycle. To record the time-dependent evolution of the velocity fields at the measured plane, the method proposed by Birch and Dickinson [47] was applied in the present study. As shown in Fig. 1b, a rotational platform was applied to modulate the time when the measured plane coincides with the laser sheet. Based on the method, we can obtain the time-dependent evolution of the LEV at a given span location. Owing to the 3D structure of LEVs, the flow fields at fourteen span loca-

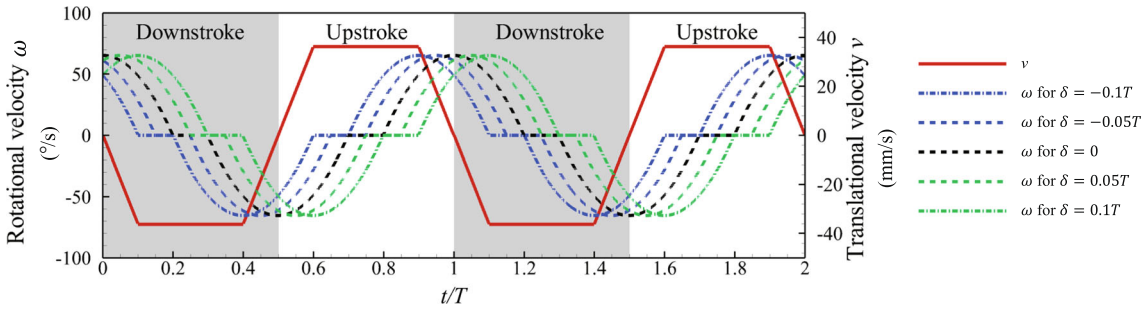

Fig. 2 Wing kinematics of the robotic fly in our experiments by referring to the experiments of Dickinson et al. [4]. Solid red line indicates the translational (stroke) velocity of the wing, dashed and dash-dot lines indicate the rotational (pitch) velocity of the wing. The stroking amplitude is 120°, the angle of attack at the middle of downstroke is 40°, and the angle of attack at the middle of downstroke is 20°

tions were measured in the present study. The time interval between the two images was 5000 μs, which guarantees that the particles will be not out of the laser sheet. The recorded region has 2320×1200 pixels with a spatial field of view of 333×170 mm^2. The obtained images were paired and processed by a commercial software called Fluere, which applies the cross-correlation algorithm. The interrogation areas were 32×32 pixels windows with 50% overlap. After the velocity fields were obtained, a second-order accurate scheme was employed to calculate the vorticity fields with the finite differences in velocity data with eight neighboring points. By satisfying the constraints of PIV measurements (interval time, particle size, and particles concentration), the uncertainties in the velocity measurement and vorticity calculation were less than 1% and 3%, respectively [48].

2.2 Wing kinematics of robotic fly

The wing kinematics is similar to "∞", which consists of three motions: translation (stroke), rotation (pitch), and deviation from the stroke plane (deviation). Although the wing deviation has an influence on the aerodynamics of flapping wing, the most significant contribution to the aerodynamic forces is the coordinative motion of the wing translation and wing rotation [4].

As shown in Fig. 2 and also explained by Dickinson et al. [4], the downstroke or upstroke process of the flapping wing is typically divided into three portions including (i) translational acceleration and pitching-down rotation at the beginning of the stroke; (ii) translation at a constant speed and constant pitch angle during the middle of the stroke; (iii) translation deceleration and pitching-up rotation at the end of the stroke. Thus, the wing kinematics of the robotic fly were designed to replay the three portions. The translational velocity (denoted by v) of the wing geometric center and the rotational velocity (denoted by ω) of wing in our experiments are shown in Fig. 2. When the wing pitches up and down, the variation of ω satisfies the sinusoidal function. When v is accelerated or decelerated, the acceleration or deceleration are constant. Besides, the duration time of one stroke cycle is $T = 6$ s.

According to the analysis of wing kinematics of fruit fly [44], the phase shift δ between stroke reversal and wing rotation plays an important role when fruit fly steers maneuvers. In order to investigate the influence of wing rotation mode on the formation of LEV, five sets of experiments including two advanced modes ($\delta < 0$), a symmetrical mode ($\delta = 0$), and two delayed modes ($\delta > 0$), are performed in our study and shown in Fig. 2. The five cases are $\delta = -0.1T$, $\delta = -0.05T$, $\delta = 0$, $\delta = 0.05T$, and $\delta = 0.1T$, respectively. In addition, referring to the experiments of Dickinson et al. [4] and according to the real wing kinematics observed by Fry et al. [44], both the flapping amplitude (including the stroking and rotating amplitude) and flapping frequency are fixed in the presented study to satisfy that the Reynolds number of hovering flight is approximately 240.

3 Evolution of flow pattern and the leading-edge vortex

3.1 Evolution of the flow pattern around the flapping wing

Figure 3 shows the evolution of the flow pattern in a whole stroke cycle, which consists of a downstroke phase ($0 < t < 0.5T$) and an upstroke phase ($0.5T < t < 1.0T$), for the advanced mode $\delta = -0.1T$. At the beginning of downstroke ($t/T = 0.02$), the wing has rotated for a period of time and interacts with the vortices generated by the previous stroke. When $t/T = 0.131$, the vortices generated by the previous stroke are shed into the wake and new vorticity is produced from the boundary layer of the wing. At $t/T = 0.37$, the flow separates at the leading edge of wing, generating a patch of high negative vorticity (clockwise spin) named LEV. At the trailing edge of the wing, positive vorticity is produced and

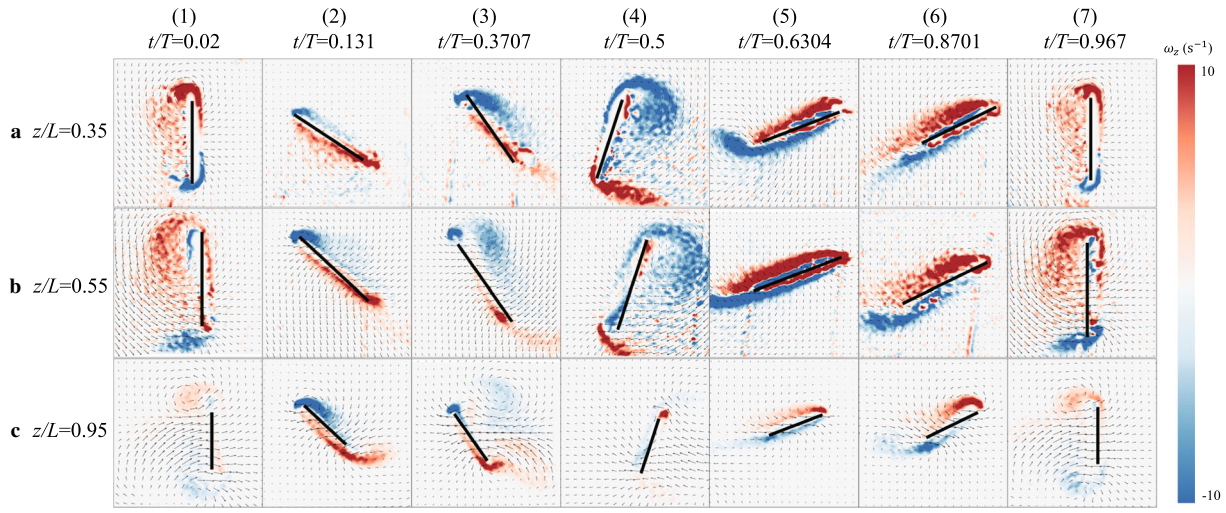

Fig. 3 Contours of the flow structures around the wing for the advanced mode $\delta = -0.1T$. Plots (1)–(7) show the flow contours at different instants and plots **a**–**c** show the streamwise flow fields at three spanwise locations. The spanwise locations are 35%, 55%, and 95% of the semi-wingspan for plots **a**–**c**, respectively. That is, plots **a**–**c** show the flow contours in root, mid-span, and tip regions of the wing. The fields were measured during the fourth stroke. The solid lines indicate the position and attack angle of the wing. Black circles indicate the leading edge of the wing

sheds into the wake. Comparison of the flow contours at the three spanwise locations demonstrates that the size of LEV at midspan location is the largest, and the vorticity of LEV at the tip region is downstream transported owing to the formation of tip vortex. Besides, the size of LEV at the mid-span and root of the wing is strong enough to prevent positive vorticity at the trailing edge of the wing from rolling up to form a trailing vortex (TRV), whereas the positive vorticity rolls up to form the TRV at the tip region of the wing. When the wing rotates at the end of downstroke ($t/T = 0.5$), the formation of the LEV is further enhanced, but the LEV still remains stable attached on the wing, which is also observed by Lentink and Dickinson [14]. During wing rotation process, the wing passes through the LEV and recaptures the energy of LEV, as shown in Figs. 3**a**-(4) and **b**-(4). This mechanism is termed wake capture, which plays a significant role in the generation of lift [4]. From $t/T = 0.63$ to $t/T = 0.967$, the upstroke phase is performed, in which the evolution of flow contour is similar to that in downstroke phase. By comparing the contours of LEVs at the end of the upstroke or downstroke, one can find that both the size and strength of LEV generated in the upstroke are slightly smaller than those of the LEV generated in the downstroke, as shown in Figs. 3, 4, and 7.

Figures 4 and 5 show the evolution of flow patterns during one whole stroke cycle for the symmetric mode $\delta = 0$ and the delayed mode $\delta = 0.1T$, respectively. Compared with the flow patterns for the advanced mode, one can find some obvious differences as follows. At the beginning of downstroke ($t/T = 0.02$), the wake vortices generated by the previous stroke are the strongest for the advanced mode and the weakest for the delayed mode. From $t = 0.131T$ to $t = 0.37T$, LEVs grow at the leading edge of wing for the three modes, but the growth rate of LEV for the delayed mode seems to be the largest. These LEVs are stably attached on the wing, and the span distributions of their vorticity are similar. From $t = 0.37T$ to $t = 0.5T$, the LEV for the advanced mode further grows (Fig. 3); however, the LEVs for the symmetric and delayed modes exhibit no longer growth (Figs. 4 and 5). As a result, the LEV generated by the flapping wing with advanced mode has the largest size at the end of stroke, as shown in Figs. 3–5. Moreover, for the delayed mode, the LEV and the trailing vortex at the tip region separate from the wing. From the flow patterns, one can find that the orientation between the LEV and the wing is changed by the mode of wing rotation. Thus, the mode of wing rotation plays an essential role in the wake capture mechanism. From $t = 0.5T$ to $t = 0.63T$, the wing stroke is reversing and the wing is rotating, generating rotational circulation and wake capture mechanism, as shown in Figs. 3–5. From $t = 0.63T$ to $t = 0.967T$, the upstroke process is performed.

3.2 Circulation distribution and evolution of leading-edge vortex

During a stroke cycle, two separated LEVs (Labelled LEV1 and LEV2) roll up on the upper surface of wings during the downstroke and upstroke, respectively. To investigate the formation of LEV, the circulation of LEV at each spanwise section is estimated by using Stokes' theorem:

$$\Gamma = \iint_A \omega_z \mathrm{d}A, \tag{2}$$

where the area A was determined in each time step to encompass the vortex of interest, in which the vorticity is larger than 5% of the maximal vorticity magnitude in the LEVs.

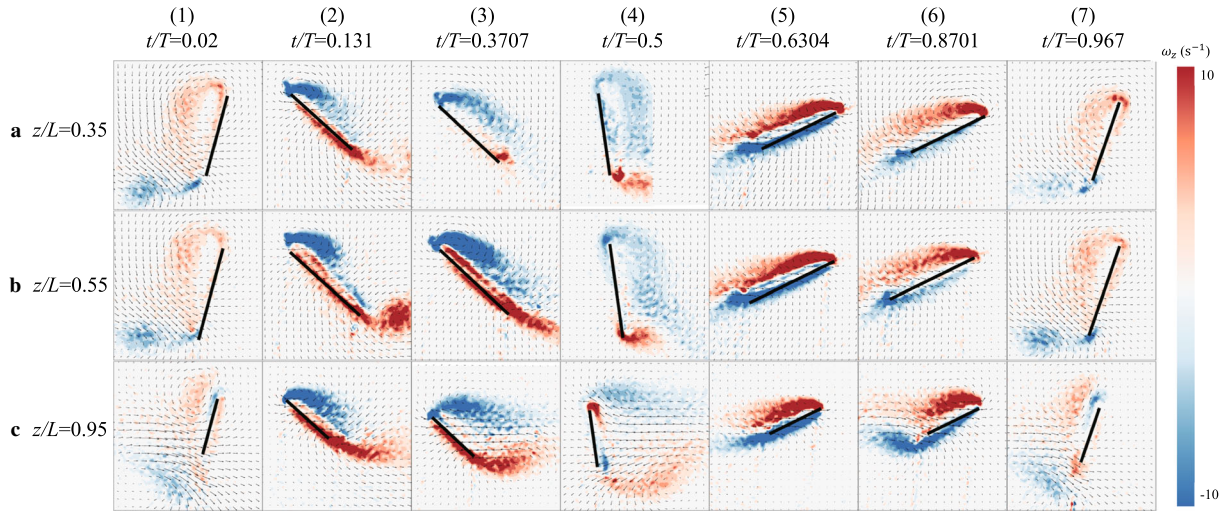

Fig. 4 Contours of the flow structures around the wing for the symmetric mode $\delta = 0$. Plots (1)—(7) show the flow contours at different instants and plots **a**–**c** show the streamwise measurements at different positions along the span. The span locations are 35%, 55%, and 95% of the semi-wingspan for plots **a**–**c**, respectively. That is, plots **a**–**c** show the flow contours in root, mid-span, and tip regions of the wing. The fields were measured for the fourth stroke. The solid lines indicate position and attack angle of the wing. The black circle indicates the leading edge of the wing

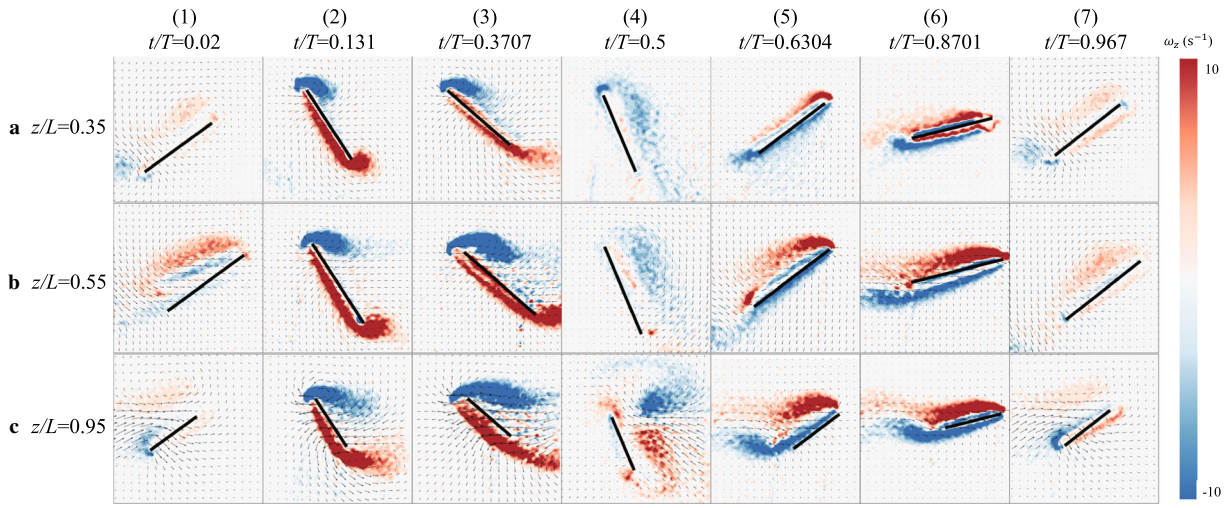

Fig. 5 Contours of the flow structures around the wing for the delayed mode $\delta = 0.1T$. Plots (1)–(7) show the flow contours at different instants and plots **a**–**c** show the streamwise measurements at different positions along the span. The span locations are 35%, 55%, and 95% of the semi-wingspan for plots **a**–**c**, respectively. That is, plots **a**–**c** show the flow contours in root, mid-span, and tip regions of the wing. The fields were measured for the fourth stroke. The solid lines indicate position and attack angle of the wing. The black circle indicates the leading edge of the wing

The choice of 5% threshold not only can filter out the background noises in PIV measurement, but also can distinguish the region of LEV from the flow contour with very small uncertainty.

Figure 6 shows the spanwise circulation of the two LEVs for the advanced mode $\delta = -0.1T$, symmetric mode $\delta = 0$, and delayed mode $\delta = 0.1T$. During the wing revolving process, the tangential velocity along the span of wing from the root to the wingtip increases. As a result, the spanwise circulation of LEVs generally exhibits an increased tendency from the root to the wingtip. However, the circulation of LEV in the wingtip region decreases obviously, largely because of the vorticity transport induced by the formation of the wingtip vortex. For $\delta = 0$ and $\delta = 0.1T$, the span distribution of LEV circulation is nearly identical with that for $\delta = -0.1T$, as shown in Fig. 6a–c. The main difference is that the wingtip vortex has a more significant influence on the LEV for $\delta = -0.1T$ than those for $\delta = 0$ and $\delta = 0.1T$. The influence area of the wingtip vortex on the circulation of LEV is the largest for $\delta = -0.1T$, which can also be observed through the flow contours in Figs. 3–5.

In the wake of flapping flight (shown in Figs. 3–5), the persistent LEV with stable attachment on the wing is the key feature and the TRV rolls up at the trailing edge of the

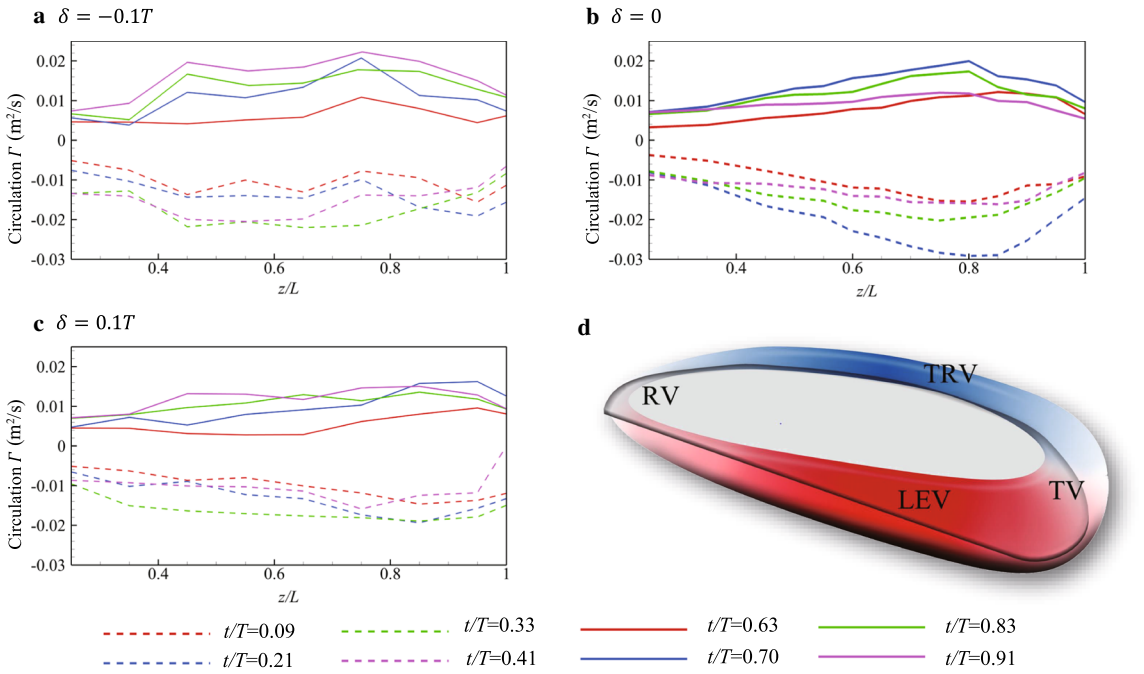

Fig. 6 **a**–**c** Spanwise distribution of circulation of LEVs for **a** the advanced mode $\delta = -0.1T$, **b** the symmetric mode $\delta = 0$, and **c** the delayed mode $\delta = 0.1T$. The dashed and solid lines indicate the LEV1 and LEV2 generated by the downstroke and upstroke, respectively. The red, blue, green, and purple dashed lines correspond to the times at $t/T = 0.09$, $t/T = 0.21$, $t/T = 0.33$, and $t/T = 0.41$, respectively. The red, blue, green, and purple solid lines correspond to the times at $t/T = 0.63$, $t/T = 0.70$, $t/T = 0.83$, and $t/T = 0.91$, respectively. **d** Cartoon of the vortex loop around the flapping wing. The depth of the color represents the magnitude of vorticity

wing. Owing to the pressure difference between the upper and below surface of wing, a tip vortex (TV) forms in the wingtip region and weakens the strength of the LEV at the wingtip region. At the corner area between the root of wing and the body of robotic model, a root vortex (RV) inevitably forms. Therefore, a vortex loop model, which consists of the LEV connected to the TRV via a TV and a RV, is suggested to describe the vortex structure around the flapping wing, as shown in Fig. 6d.

In the vortex loop, of particular importance to aerodynamic forces is the presence of LEVs, whose formation explains the enhancement of lift at a high angle of attack and an instantaneous peak of lift at the beginning of wing rotation (shown in the results of Dickinson et al. [4]). Thus, we would like to investigate the circulation evolution of LEVs.

In Fig. 7, the circulation growth of LEV1 and LEV2 at different spanwise locations is shown for the three modes of wing rotation. It is found that the circulation of LEV exhibits a non-linear growth with the stroke of wing. As shown in Fig. 7a, the circulation of LEV at the spanwise location from $z/L = 0$ to $z/L = 0.75$ increases in the whole downstroke and upstroke, whereas the circulation at the wingtip region from $z/L = 0.85$ to $z/L = 1$ no longer grows and even decreases after $t \approx 0.2T$. The circulation evolution of LEV for the three modes at the wingtip region exhibits a similar tendency. That is, the circulation increases for a period of time and then decreases due to vorticity transport induced by the wingtip vortex. By comparing the peak strength of LEVs for the three modes, one can find that LEV1's circulation reaches the peak at $t/T \approx 0.44$ for advanced mode, whereas LEV1's circulation reaches the peak at much earlier time for symmetrical and delayed modes, corresponding to $t/T \approx 0.25$ and $t/T \approx 0.2$, respectively. This indicates that the decaying wing rotation is useful to increase the growth rate of LEV circulation. By comparing the peak circulation of LEV, it is found that the strength of LEVs for the advanced mode is larger than these for the symmetrical and delayed modes. This suggests that advancing wing rotation can enhance LEV's formation, whereas delaying wing rotation constrains LEV's formation.

Based on the above investigation, a diagrammatic cartoon is drawn in Fig. 8 to qualitatively explain the role of wing rotation in the formation of LEV. If the wing rotation precedes stroke reversal, the wing can capture the vortices (LEV0 in downstroke and LEV1 in upstroke) at a positive angle that produces positive lift, as shown in Fig. 8a. If the wing rotation is symmetrical or delayed with stroke reversal, the wing is arranged with a negative angle, resulting in no lift and negative lift, as shown in Fig. 8b, c. The strength of LEV is also modulated by the wing rotation. Stronger LEV is generated by advancing wing rotation and smaller LEV is generated by delaying wing rotation. Besides, the growth rate of LEV can be increased by advancing the wing rotation. Therefore, wing

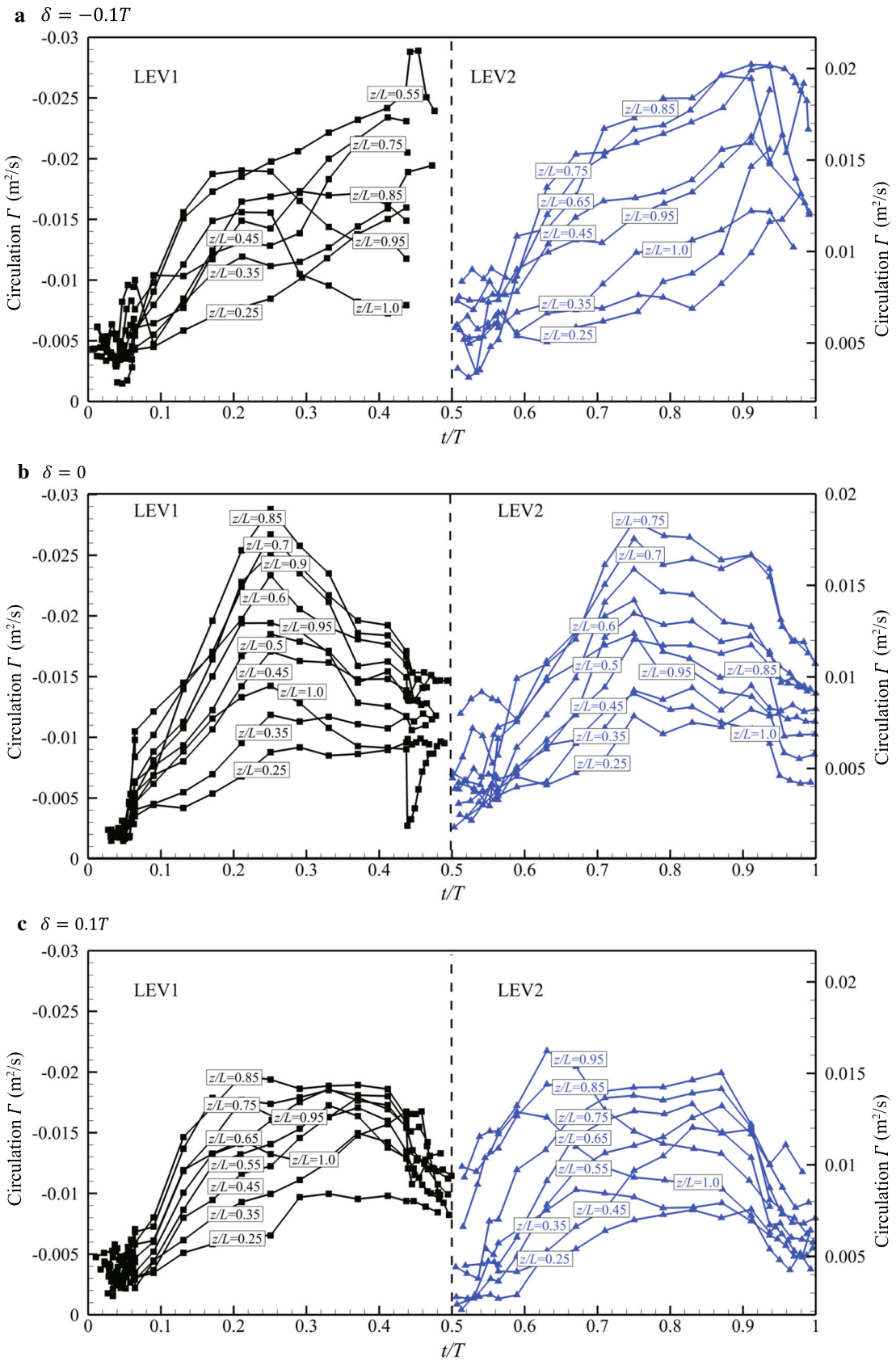

Fig. 7 Circulation evolution of LEVs generated by the downstroke and upstroke for **a** the advanced mode $\delta = 0.1T$, **b** the symmetric mode $\delta = 0$, and **c** the delayed mode $\delta = 0.1T$

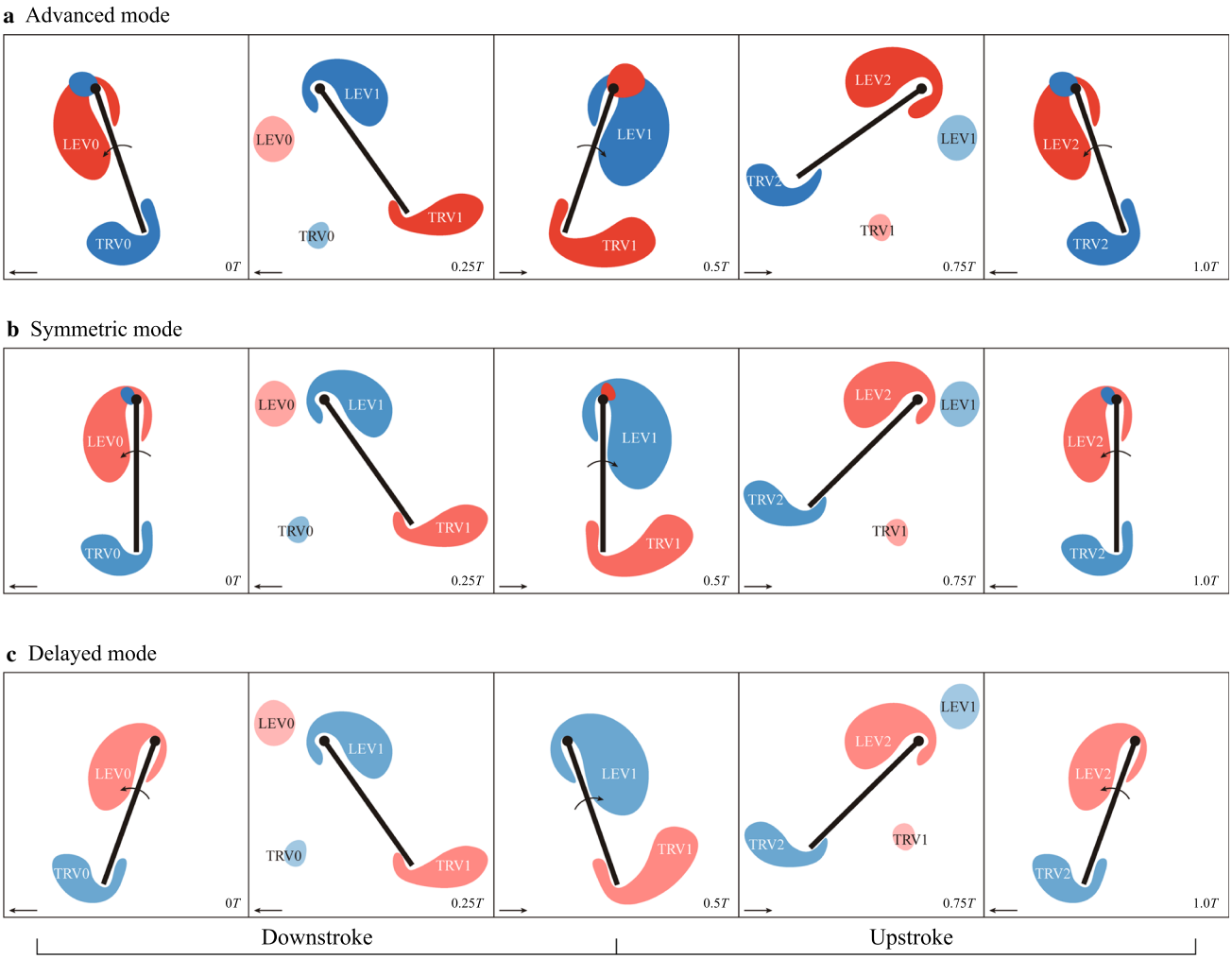

Fig. 8 Diagram of the flow patterns obtained by different modes of wing rotation. The line represents the wing chord, with the circle indicating the leading edge. Warm tones (reds) represent counter-clockwise vorticity; cool tones (blues) represent clockwise vorticity. The depth of colour reflects the strength of vortices. The arrows on the line and in the bottom of each subfigure indicate the moving and rotational direction of the wing, respectively

rotation can accelerate or hinder the formation of LEV, and wing rotation actually has changed the characteristic length scale that feeds the formation of LEV and has an important role in the scaling formation number of LEV.

4 Scaling formation number of leading-edge vortex

With the presentation of the LEV formation, we intend to investigate the scaling formation number of the 3D LEV generated by the flapping wing, based on the idea of vortex formation time originally developed for vortex ring formation and proposed by Gharib et al. [32]. Based on the vorticity production mechanism of a vortex, the formation time T^* of a vortex is defined in a general form as the following manner [33,49]:

$$T^* = \frac{C\Gamma}{D\Delta U}, \tag{3}$$

where Γ is the circulation of the vortex, D is the characteristic length scale, C is the constant factor depending on the physical configuration of the vortex generator, and ΔU is the strength of the shear-layer feeding velocity.

As is well-known, the motion of the wing at each spanwise location can be described by the coordinative motion of pitching and plunging of the wing. Moreover, the study of the pitching and plunging plate or wing is the canonical and fundamental problem to understand the flapping flight. In the studies of Rival et al. [13] and Onoue and Breuer [20], the formation time of the LEV generated by the pitching and plunging plate/wing is also defined as Eq. (3). In their study, the characteristic length scale is set as $D = 2c$, where c is the chord length. The shear-layer feeding velocity was approximated by $\Delta U = 2\,\pi\, fl$, where f is the flapping fre-

quency and l is the span distance to the root of the wing. The constant factor C is set to 1.0. Thus, we also applied the definitions in the presented study by referring to the definitions of the studies of Rival et al. [13] and Onoue and Breuer [20]. Remaining consistence with their definitions is also helpful for us to compare the our results with theirs.

In addition to the above definition based on vortex circulation, the formation time of a vortex can also be determined by the kinematics of the vortex generator. Such as, the formation time of vortex rings generated by the piston-cylinder apparatus is originally defined as the ratio of the stroke length of piston to the diameter of piston. By referring to definition of the formation time for the vortex rings, Milano and Gharib [50] proposed another definition of formation time of the 2D LEV at a given spanwise location. During one cycle, two LEVs with the opposite vorticity are generated in the downstroke and upstroke, respectively. Thus, the formation times T^{**} based on wing kinematics for the two LEVs generated by the downstroke and upstroke are respectively calculated by

$$\begin{cases} T^{**} = |\int_0^t \frac{v(t)+\frac{1}{2}c\omega(t)\sin[\alpha(t)]}{c\sin[\alpha(t)]}\mathrm{d}t|, \text{ with } \quad t \le 0.5T, \\ T^{**} = \int_{0.5T}^t \frac{v(t)+\frac{1}{2}c\omega(t)\sin[\alpha(t)]}{c\sin[\alpha(t)]}\mathrm{d}t, \text{ with } \quad t > 0.5T, \end{cases} \tag{4}$$

where $v(t)$ is the translational velocity, $\omega(t)$ is the angular velocity of wing rotation, and $\alpha(t)$ is the time-dependent attack angle. In Eq. (4), the term of $v(t) + \frac{1}{2}c\omega(t)\sin[\alpha(t)]$ indicates the wing stroke length (similar to the piston stroking length), and the term of $c\sin[\alpha(t)]$ indicates the scaling length feeding the growth of LEV (similar to the piston diameter). Moreover, the scaling length is the projected length of the chord perpendicular to the direction of wing translation. Owing to the change of attack angle during wing rotation, the scaling length is changed and is $c\sin[\alpha(t)]$.

By using experimental measurements and in terms of the commanded wing kinematics, we can obtain the formation time ($T^*(z)$ and $T^{**}(z)$) of the LEV at each spanwise location. Owing to the spanwise distribution of the 3D LEV's circulation, the modifications for the two definitions of vortex formation time are given as

$$T^*_{\mathrm{LEV}} = \frac{\int_0^L T^*(z)c\mathrm{d}z}{S}, \tag{5}$$

$$T^{**}_{\mathrm{LEV}} = \frac{\int_0^L T^{**}(z)c\mathrm{d}z}{S}, \tag{6}$$

where $T^*(z)$ and $T^{**}(z)$ indicate the formation time of the LEV at each spanwise location, which are determined by Eqs. (3) and (4), respectively.

Based on the Eqs. (3)–(6), the variations of T^*_{LEV} and T^{**}_{LEV} against time during one cycle are presented in Fig. 9. It is found that T^{**}_{LEV} denoted by the red lines increases during the whole stroke for the three cases. However, T^*_{LEV} denoted by the dashed lines does not increase all the time and instead decreases after T^*_{LEV} reaches the peak. This tendency indicates that the LEV no longer grows and pinches off after T^*_{LEV} reaches the peak. Intuitively, the decreasing of T^* may be owing to the deceleration of the leading-edge velocity of the wing. In the appendix, the variations of the leading-edge velocity in one cycle are shown, and one can find that the time when T^*_{LEV} decreases does not coincide with the deceleration of the leading-edge velocity. Thus, it is believed that the decreasing of the T^*_{LEV} should be owing to the pinch-off of the LEVs rather than the deceleration of the leading-edge velocity. In addition, the pinch-off of LEVs is attributed to the energy restriction implied by the Kelvin-Benjamin variational principle [32]. In particular, Onoue and Breuer investigated the energy feature of the LEVs generated by a pitching and plunging wing and successfully explained the pinch-off of the LEVs [20].

In terms of the implication of T^*_{LEV}, the peak of T^*_{LEV} is termed as the formation number of LEV (denoted by F^*). As shown in Fig. 9a–c, F^* of LEVs are 5.3, 4.8, and 3.6 (marked by the arrows) for the advanced mode $\delta = -0.1T$, symmetric mode $\delta = 0$, and delayed mode $\delta = 0.1T$, respectively. For the mode $\delta = -0.1T$, LEV reaches $F^* = 5.3$ at $t \approx 0.43T$. This phenomenon agrees with the observation shown in Fig. 3, in which the LEV still grows from $t = 0.37T$ to $t = 0.5T$. For the modes $\delta = 0$ and $\delta = 0.1T$, the formation of LEV reaches the formation number at $t = 0.23T$ and $t = 0.31T$, respectively. These phenomena can also be convinced by the formation of LEV. As shown in Figs. 4 and 5, LEVs are stretched and their strength is even reduced from $t = 0.37T$ to $t = 0.5T$. During the upstroke for the delayed mode ($\delta = 0.1T$), the T^* of LEV2 arrives the peak at $t = 0.83T$ and the peak T^* is approximately 2.5. From Fig. 5 (5)–(7), the strength of LEV indeed arrives the maximum about $t \approx 0.85T$ and then decreases. Besides, this tendency is also observed by the circulation evolution shown in Fig. 7. Therefore, the formation number of LEVs generated by the flapping wing is found to stay in the range of $2.5-5.5$, within which the formation number of the approximated 2D LEVs obtained by Rival et al. [13] and the 3D LEVs obtained by Onoue and Breuer [20] also stay. However, the range of the formation number of the LEVs in the presented study is a bit broader than the optimal vortex formation number generalized by Dabiri [33] because of the wing rotation. According to the results of Rival et al. [13] and Onoue and Breuer [20], the LEVs generated by a pitching and plunging plate begin to pinch off, convect, stretch, and separate from the plate after the LEVs reach the formation number. However, as shown in Figs. 3–5, the LEVs generated by the flapping wing at some spanwise locations still grow after the LEVs reach the formation number. As is well known, the spanwise vorticity is transported along the span of flapping wing or by the

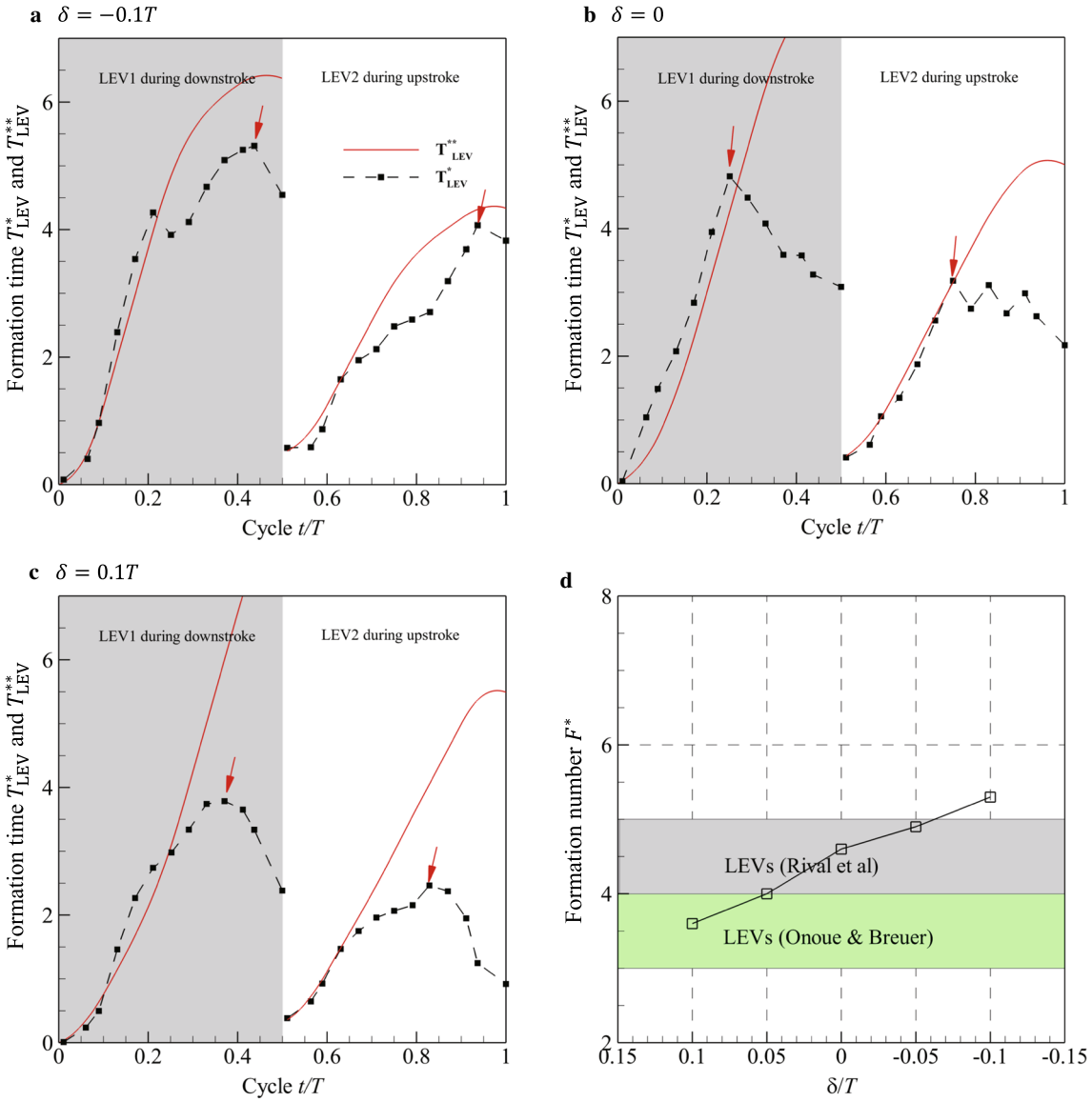

Fig. 9 Variations of T^*_{LEV} and T^{**}_{LEV} against time during one cycle for **a** the advanced mode $\delta = -0.1T$, **b** the symmetric mode $\delta = 0$, and **c** the delayed mode $\delta = 0.1T$. The red solid lines indicate the variation of T^{**}_{LEV} based on wing kinematics (Eq. (6)) and the dashed lines indicate the variation of T^*_{LEV} based on vortex circulation (Eq. (5)). **d** The variation of F^* of LEV1 generated by downstroke with δ. The value of formation number is the peak of T^*_{LEV}, marked by the red arrows in Fig. 9a–c

formation of wingtip vortex. According to the flow contours in Figs. 3, 4 and the circulation evolution in Fig. 7, one can find that spanwise vorticity is significantly transported from wing-tip region to wing-root region or into the wake by the wingtip vortex. As the result of vorticity-flux balanced mechanism, the LEVs stably remain attached on the flapping wing after the LEVs reach the formation number and shed into the wake until the next stroke happens.

In Fig. 9d, the variations of F^* with δ are presented. It is found that the phase shift of wing rotation actually plays a considerable role in the scaling formation number of LEV. Advancing wing rotation can delay the formation number of LEV, and delaying wing rotation is the opposite. Here, one question may arise that how wing rotation changes the formation number of LEV. According to the previous investigation, the formation number of vortex rings can be varied by the temporally decreasing or increasing the diameter of nozzle exit [38]. Besides, a converging nozzle can generate a vortex ring whose formation number is 2.0. Actually, wing rotation has an identical role in modulating the characteristic length scale that feeds the formation of LEV. As shown in Eq. (4), the characteristic length scale of LEV generator based on wing kinematics depends on the wing rotation. Thus, the formation number of LEVs is varied by the wing rotation and depends on the phase shift of wing rotation. Based on the implications of vortex pinch-off [51,52], a larger forma-

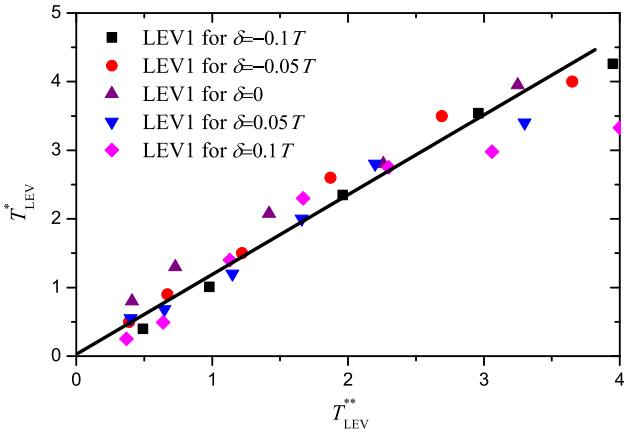

Fig. 10 Variation of T^*_{LEV} of LEV against T^{**}_{LEV} before the LEV reaches the formation number. T^*_{LEV} is the formation time based on LEV circulation, and T^{**}_{LEV} is the formation time based on wing kinematics

tion number of LEV means that the performance of flapping flight is more efficient. Therefore, insects can appropriately modulate the formation and the formation number of LEV by smart wing rotation, according to flight demand.

Based on the definitions of formation time (Eqs. (3) and (4)), T^*_{LEV} indicates the circulation formation of LEV and T^{**}_{LEV} indicates the contribution of wing kinematics to LEV formation. The corresponding values of T^{**}_{LEV} to each discrete T^*_{LEV} can be obtained from the results shown in Fig. 9a–c. Then, we plot the variation of T^*_{LEV} against T^{**}_{LEV} before $T^*_{LEV} \leq F^*$, as shown in Fig. 10. It is found that T^*_{LEV} has an approximately linear relationship with T^{**}_{LEV}. Therefore, a scaling model for predicting the circulation growth of LEV is suggested and expressed as

$$\Gamma = \tau T^{**}_{LEV} \times (D\Delta U), \qquad \text{with} \quad T^*_{LEV} \leq F^*, \tag{7}$$

where τ is approximately 1.0 and slightly depends on the mode of wing rotation. Combining Eqs. (4), (6), and (7), one can predict the circulation growth of LEV on a flapping wing based on the wing kinematics. Besides, the maximum of LEV circulation can be described by the optimal formation number. When the LEVs obtain the maximal circulation at the formation number, the vorticity of LEVs is transported by the spanwise flow, wingtip vortex and other mechanisms. As a result, the circulation of LEVs no longer grows and even slightly decreases after the LEVs reach the formation number.

5 Conclusions

In this paper, an experiment of a robotic model at Reynolds number of approximately 240 was designed to investigate a scaling for the formation of the LEV. The time-dependent velocity fields at fourteen spanwise locations along the wing were measured by using PIV technique. Three modes of wing rotation with fixed flapping amplitude and frequency, including two advanced modes ($\delta < 0$), a symmetrical mode ($\delta = 0$), and two delayed modes ($\delta > 0$), were performed in the present study.

Experimental results demonstrated that the LEV grows on the top surface of the wing and the vortex circulation has a spanwise distribution, in which the circulation of LEV at the wing middle region is larger than that at the wing root and tip regions is smaller. A vortex loop model that consists of the 3D LEV on the top of the wing connected with the trailing vortex via a tip vortex and a root vortex, is suggested to describe the flow structure around the flapping wing. By modulating the mode of wing rotation, the formation of LEV exhibits differences. By advancing wing rotation, a stronger LEV is generated and results in a stronger wake capture mechanism. By delaying wing rotation, the growth rate of LEV is obviously improved, although the strength of LEV is smaller than that obtained by advancing wing rotation. To vividly describe the formation of LEV, a diagram cartoon is drawn.

Based on physical definition of vortex formation time, the formation time for LEVs generated by flapping wing is defined by two distinct manners. One is based on the circulation production mechanism (denoted by T^*_{LEV}). The other is based on the wing kinematics (denoted by T^{**}_{LEV}). The peak of T^*_{LEV} indicates the formation number of LEVs (denoted by F^*). It is found that the formation number of LEVs stays in the range of $2.5 - 5.5$, within which the formation number of the approximated 2D LEVs obtained by Rival et al. [13] and the 3D LEVs obtained by Onoue and Breuer [20] stay. In addition, the formation number basically agrees with the optimal vortex formation number found by Gharib et al. [32] and generalized by Dabiri [33]. As for the LEV generated by the flapping wing, advancing wing rotation can delay the formation number of LEV, and delaying wing rotation is the opposite. The underlying mechanism is greatly owing to that wing rotation with different δ changes the characteristic length scale that feeds the formation of LEV. Moreover, the LEVs stably remain attached on the flapping wing and even grows at some spanwise locations after the LEVs reach the formation number because of vorticity transport. This is quite different from the LEV generated by a pitching and plunging plate, which pinches off, convects, stretches, and even separates from the plate after the LEV reaches the formation number. Furthermore, the approximately linear relationship between T^*_{LEV} and T^{**}_{LEV} before the LEV reaches the formation number suggests that the circulation growth of LEVs exhibits a scaling law based on wing kinematics. Therefore, a model for predicting the circulation growth of LEVs generated by the flapping wing is suggested based on the scaling law.

Acknowledgements This work was supported by the State Key Development Program of Basic Research of China (Grant 2014CB744802), the National Natural Science Foundation of China Project (Grant 91941301), and the China Postdoctoral Science Foundation (Grant 2018M642007).

Appendix: Leading-edge velocity of flapping wing

For the flapping wing, the leading-edge velocity ($u(t)$) can be defined as

$$u(t) = v(t) + \frac{1}{2}c\omega(t)\sin\left[\alpha(t)\right]. \tag{A.1}$$

Figure 11 shows the variations of the leading-edge velocity of the wing during one cycle. It is found that the leading-edge velocity begins to decrease at approximately $t/T = 0.3$, $t/T = 0.4$, and $t/T = 0.4$ for $\delta = -0.1T$, $\delta = 0$, and $\delta = 0.1T$. Compared with the variation of T^* shown in Fig. 9, one can find that the decreasing of T^* does not coincide with the deceleration of the leading-edge velocity.

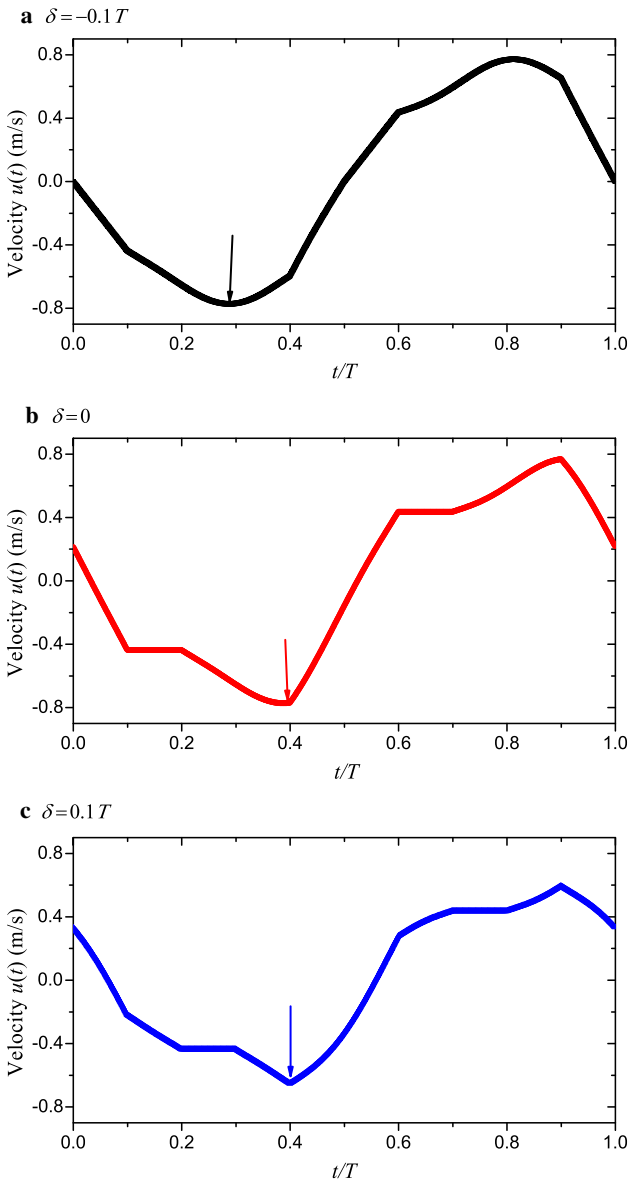

Fig. 11 Variations of the leading-edge velocity ($u(t)$) of the wing during one cycle for **a** the advanced mode $\delta = -0.1T$, **b** the symmetric mode $\delta = 0$, and **c** the delayed mode $\delta = 0.1T$. The arrows indicate the time when the leading-edge velocity begins to decelerate

References

1. Wootton, R.J.: Palaeozoic insects. Annu. Rev. Entomol. **26**, 319–344 (1981)
2. Sun, M.: Insect flight dynamics: stability and control. Rev. Mod. Phys. **86**, 615–646 (2014)
3. Birch, J.M., Dickinson, M.H.: Spanwise flow and the attachment of the leading-edge vortex on insect wings. Nature **412**, 729–733 (2001)
4. Dickinson, M.H., Lehmann, F.O., Sane, S.P.: Wing rotation and the aero-dynamic basis of insect light. Science **284**, 1954–1999 (1999)
5. Chen, L., Wu, J., Cheng, B.: Leading-edge vortex formation and transient lift generation on a revolving wing at low Reynolds number. Aero. Sci. Technol. **97**, 105589 (2020)
6. Nakata, T., Noda, R., Kumagai, S., et al.: A simulation-based study on longitudinal gust response of flexible flapping wings. Acta Mech. Sin. **34**, 1048–1060 (2018)
7. Zhang, J.D., Huang, W.X.: On the role of vortical structures in aerodynamic performance of a hovering mosquito. Phys. Fluids **31**, 051906 (2019)
8. Hirato, Y., Shen, M., Gopalarathnam, A., et al.: Flow criticality governs leading-edge-vortex initiation on finite wings in unsteady flow. J. Fluid Mech. **910**, A1 (2021)
9. Werner, N.H., Chung, H., Wang, J., et al.: Radial planetary vorticity tilting in the leading-edge vortex of revolving wings. Phys. Fluids **31**, 041902 (2019)
10. Harbig, R.R., Sheridan, J., Thompson, M.C.: Reynolds number and aspect ratio effects on the leading-edge vortex for rotating insect wing planforms. J. Fluid Mech. **370**, 166–192 (2013)
11. Jardin, T.: Coriolis effect and the attachment of the leading edge vortex. J. Fluid Mech. **820**, 312–340 (2017)
12. Ellington, C.P.: The aerodynamics of hovering insect flight i–iv. Philos. Trans. R. Soc. Lond. Ser. B. **305**, 1–81 (1984)
13. Rival, D., Prangemeier, T., Tropea, C.: The influence of airfoil kinematics on the formation of leading-edge vortices in bio-inspired flight. Exp. Fluids. **46**, 823–833 (2009)
14. Lentink, D., Dickinson, M.H.: Rotational accelerations stabilize leading edge vortices on revolving *y* wings. J. Exp. Biol. **212**, 2705–2719 (2009)
15. Smith, L.R., Jones, A.R.: Vortex formation on a pitching aerofoil at high surging amplitudes. J. Fluid Mech. **905**, A22 (2020)
16. Wong, J.G., Rival, D.E.: Determining the relative stability of leading-edge vortices on nominally two-dimensional flapping profiles. J. Fluid Mech. **766**, 611–625 (2015)
17. Fu, J.J., Heer, C., Qiu, H.H., et al.: Effects of aspect ratio on, flapping wing aerodynamics in animal flight. Acta Mech. Sin. **30**, 776–786 (2015)
18. Chen, L., Zhou, C., Wu, J.: The role of effective angle of attack in hovering pitching-flapping-perturbed revolving wings at low Reynolds number. Phys. Fluids **32**, 011906 (2020)

19. Onoue, K., Breuer, K.S.: Vortex formation and shedding from a cyber-physical pitching plate. J. Fluid Mech. **793**, 229–247 (2016)
20. Onoue, K., Breuer, K.S.: A scaling for vortex formation on swept and unswept pitching wings. J. Fluid Mech. **832**, 697 (2017)
21. Eldredge, J.D., Jones, A.R.: Leading-edge vortices: mechanics and modeling. Annu. Rev. Fluid Mech. **51**, 75 (2019)
22. Sarkar, S., Chajjed, S., Krishnan, A.: Study of asymmetric hovering in flapping flight. Eur. J. Mech. B/Fluids **37**, 72–89 (2013)
23. Chen, M.W., Sun, M.: Wing/body kinematics measurement and force and moment analyses of the take-off flight of fruit flies. Acta Mech. Sin. **30**, 495–506 (2014)
24. Nguyen, A.T., Le, V.D.T., Tran, T.H., et al.: Study of vertically ascending flight of a hawkmoth model. Acta Mech. Sin. **36**, 1031–1045 (2020)
25. Beem, H.R., Rival, D.E., Triantafyllou, M.S.: On the stabilization of leading-edge vortices with spanwise flow. Exp. Fluids. **52**, 511–17 (2011)
26. Li, Z.Y., Feng, L.H., Kissing, J., et al.: Experimental investigation on the leading-edge vortex formation and detachment mechanism of a pitching and plunging plate. J. Fluid Mech. **901**, A17 (2020)
27. Wang, C., Eldredge, J.D.: Low-order phenomenological modeling of leading-edge vortex formation. Theor. Comput. Fluid Dyn. **27**, 577–598 (2012)
28. Pitt Ford, C.W., Babinsky, H.: Lift and the leading-edge vortex. J. Fluid Mech. **720**, 280–313 (2013)
29. Xu, L., Nitsche, M.: Scaling behaviour in impulsively started viscous flow past a finite flat plate. J. Fluid Mech. **756**, 689–715 (2014)
30. Chen, D., Kolomenskiy, D., Onishi, R., et al.: Versatile reduced-order model of leading-edge vortices on rotary wings. Phys. Rev. Fluids **3**, 114703 (2018)
31. Werner, N.H., Wang, J., Dong, H., et al.: Scaling the vorticity dynamics in the leading-edge vortices of revolving wings with two directional length scales. Phys. Fluids **32**, 121903 (2020)
32. Gharib, M., Rambod, E., Shari, K.: A universal time scale for vortex ring formation. J. Fluid Mech. **360**, 121–140 (1998)
33. Dabiri, J.O.: Optimal vortex formation as a unifying principle in biological propulsion. Annu. Rev. Fluid Mech. **41**, 17–33 (2009)
34. Xiang, Y., Liu, H., Qin, S.Y.: A unified energy feature of vortex rings for identifying the pinch mechanism. ASME J. Fluid Eng. **140**, 011203 (2018)
35. Ringuette, M.J., Milano, M., Gharib, M.: Role of the tip vortex in the force generation of low-aspect-ration normal flat plates. J. Fluid Mech. **581**, 453–468 (2007)
36. Jeon, D., Gharib, M.: On the relationship between the vortex formation process an cylinder wake vortex patterns. J. Fluid Mech. **519**, 161–181 (2004)
37. Xiang, Y., Qin, S.Y., Liu, H.: Patterns for efficient propulsion during the energy evolution of vortex rings. Eur. J. Mech./B-Fluid. **71**, 47–48 (2018)
38. Dabiri, J.O., Gharib, M.: Starting flow through nozzle with temporally variable exit diameter. J. Fluid Mech. **538**, 111–136 (2005)
39. Qin, L., Xiang, Y., Lin, H.Y., et al.: Formation and dynamics of compressible vortex rings generated by a shock tube. Exp. Fluids **61**, 86 (2020)
40. Lin, H., Xiang, Y., Xu, H., et al.: Passive scalar mixing induced by the formation of compressible vortex rings. Acta Mech. Sin. **36**, 1258–1274 (2020)
41. Gao, L., Yu, S.C.M.: A model for the pinch-off process of the leading vortex ring in a starting jet. J. Fluid Mech. **656**, 205–222 (2010)
42. Rival, D.E., Kriegseis, J., Schaub, P., et al.: Characteristic length scales for vortex detachment on plunging profiles with varying leading-edge geometry. Exp. Fluids **55**, 1660 (2014)
43. Phillips, N., Knowles, K., Bomphrey, R.J.: The effect of aspect ratio on the leading-edge vortex over an insect-like flapping wing. Bioinspir Biomim. **10**, 056020 (2015)
44. Fry, S.N., Sayaman, R., Dickinson, M.H.: The aerodynamics of free-flight maneuvers in drosophila. Science **300**, 495–498 (2003)
45. Sun, M., Wu, J.H.: Aerodynamic force generation and power requirement in forward flight in a fruit fly with modeled wing motion. J. Exp. Biol. **206**, 3065–3083 (2003)
46. Gravish, N., Peters, J.M., Combes, S.A., et al.: Collective flow enhancement by tandem flapping wings. Phys. Rev. Lett. **115**, 188101 (2015)
47. Birch, J.M., Dickinson, M.H.: The influence of wing-wake interactions on the production of aerodynamic forces in flapping flight. J. Exp. Biol. **206**, 2257 (2003)
48. Qin, S.Y., Liu, H., Xiang, Y.: On the formation modes in vortex interaction for multiple co-axial co-rotating vortex rings. Phys. Fluids. **30**, 011901 (2018)
49. Gao, L., Guo, H.F., Yu, S.C.M.: A general definition of formation time for starting jets and forced plumes at low Richardson number. J. Fluid Mech. **886**, A6 (2020)
50. Milano, M., Gharib, M.: Uncovering the physics of flapping flat plates with artificial evolution. J. Fluid Mech. **534**, 403–409 (2005)
51. Krueger, P.S., Gharib, M.: The significance of vortex ring formation to the impulse and thrust of a starting jet. Phys. Fluids. **15**, 1271–1281 (2003)
52. Whittlesey, R.W., Dabiri, J.O.: Optimal vortex formation in a self-propelled vehicle. J. Fluid Mech. **737**, 78–104 (2013)